Symposuim on Biological Applications of Magnetic Nanostructures

Sarah Majetich, Chairman

Biological applications of multifunctional magnetic nanowires (invited)

D. H. Reich,[a] M. Tanase, and A. Hultgren
Department of Physics and Astronomy, Johns Hopkins University, Baltimore, Maryland 21218

L. A. Bauer
Department of Chemistry, Johns Hopkins University, Baltimore, Maryland 21218

C. S. Chen
Department of Biomedical Engineering, Johns Hopkins University, Baltimore, Maryland 21218

G. J. Meyer
Departments of Chemistry and Materials Science and Engineering, Johns Hopkins University, Baltimore, Maryland 21218

(Presented on 13 November 2002)

Magnetic particles that can be bound to cells and biomolecules have become an important tool for the application of force in biology and biotechnology. Multifunctional magnetic nanowires fabricated by electrochemical deposition in nanoporous templates are a type of magnetic carrier that offers significant potential advantages over commercially available magnetic particles. Recent experimental work aimed at developing these wires for this purpose is reviewed. Results on chemical functionalization of Au and Au/Ni wires and magnetic manipulation of wires in suspension are described. Fluorescence microscopy was used to demonstrate the covalent binding of thiol-terminated porphyrins to Au nanowires, and to optimize functionalization of two-segment gold–nickel nanowires for selectivity and stability of the nanowire–molecule linkages. Magnetic trapping is a technique where single nanowires are captured from fluid suspension using lithographically patterned micromagnets. The influence of an external magnetic field on this process is described. The dynamics of magnetic trapping is shown to be well described by a model based on the interplay of dipolar forces and viscous drag. © *2003 American Institute of Physics.*
[DOI: 10.1063/1.1558672]

I. INTRODUCTION

The integration of biology and the physical sciences at the micro- and nanoscales has the potential for impact in many areas of science and technology. One area that is particularly promising is the use of nanoengineered magnetic particles to selectively manipulate and probe biological systems. This field of biomagnetics is growing rapidly, and there is already a broad range of applications including cell separation,[1–5] biosensing,[6] studies of cellular function,[7,8] as well as a variety of potential medical and therapeutic uses.[9] The magnetic particles used to date are generally spherical, consisting of a single magnetic species and a suitable coating to allow functionalization with bioactive ligands. As the use of magnetic particles in biotechnology expands, it will become increasingly important to have magnetic carrier particles that perform a variety of functions beyond the basic one of applying force. One type of particle with significant potential in this area is electrodeposited magnetic nanowires. These are high-aspect ratio metal cylinders grown in nanoporous templates. Their radius may be tuned in the range $5 \leqslant r \leqslant 500$ nm, and they may be made up to ≈ 60 μm in length. It is possible to modulate precisely the composition along the length of the wire, which in turn enables precise control of their architecture and magnetic properties.[10] In addition, by using ligands that bind selectively to different segments of a multicomponent wire, it is possible to introduce spatially modulated multiple functionalization in these wires. This combination of features can potentially give nanowires improved performance in biomagnetic applications. In this article, we report recent advances in two areas crucial to enabling the use of magnetic nanowires in biotechnology: Control of selective functionalization of multisegment nanowires, and the ability to manipulate and control the nanowires in suspension.

The most direct approach to functionalizing multicomponent nanowires is to transfer the well-developed surface chemistry at planar metal interfaces[11] to the nanowire geometry. For example, Natan and co-workers[12] have demonstrated selective chemistry with nonmagnetic gold–platinum nanowires. For magnetic wires, we have previously shown

[a]Electronic mail: dhr@pha.jhu.edu

 © 2003 American Institute of Physics

Downloaded 13 May 2003 to 128.220.233.88. Redistribution subject to AIP license or copyright, see http://ojps.aip.org/japo/japcr.jsp

that porphyrins with terminal carboxylic acid groups bind selectively to the native oxide on Ni in single-component Ni wires,[13] and in two-component gold–nickel nanowires.[14] Porphyrins were chosen as they can be highly fluorescent and also perform important biological functions, such as catalysis and dioxygen transport, when metallated with iron.[15] Herein, we describe two results that advance the ability to control and tune the functionalization of Au/Ni nanowires. First, we have demonstrated the binding and measured the optical properties of porphyrins covalently bound to Au nanowires. This will enable the fabrication of magnetic carriers with spatially separated fluorescent segments. Second, we have optimized the functionalization of two-segment gold–nickel nanowires for selectivity and stability of the nanowire–molecule linkages.

Nanowires are good candidates for applying force to cells and biomolecules. Indeed, we have shown that ferromagnetic Ni nanowires can be bound to mammalian cells and, in some cases, outperform the commonly used superparamagnetic beads in cell sorting applications.[16] Due to their large aspect ratios, ferromagnetic nanowires have large remnant magnetizations, and hence can be used in low-field environments where the superparamagnetic beads do not perform at all. For example, we have shown that it is possible to control the self-assembly of ordered structures of magnetic nanowires from a liquid suspension with small external magnetic fields.[17] This technique has the potential for controlled assembly of cell populations in specific geometries. Another potential low-field application is the controlled manipulation of cells and nanowires using a combination of externally applied magnetic fields and local fields produced by lithographically patterned micromagnets. We have shown that one implementation of this approach, termed magnetic trapping, can be used as a means to study the electrical and magnetic properties of single nanowires.[17] In this article, we demonstrate control of nanowire trapping with an external field, and analyze the dynamics of the trapping process.

II. NANOWIRE SYNTHESIS

Single-segment Ni and Au nanowires and two-segment Ni/Au nanowires were electrodeposited into the pores of 50 μm thick alumina templates (Anodisc, Whatman) with 0.1 μm nominal pore size. A copper film was sputter deposited on one side of the template, and served as the working electrode in a three-electrode electrodeposition cell. Initially, a small amount of copper (3 C) was electrodeposited from a 1 M $CuSO_4 \cdot 5H_2O$ aqueous solution at 1.0 V to fill the ends of the nanopores. Nickel was electrodeposited from a 20 g L^{-1} $NiCl_2 \cdot H_2O$, 515 g L^{-1} $Ni(H_2NSO_3)_2 \cdot 4H_2O$, and 20 g L^{-1} H_3BO_3 aqueous solution at 1.0 V. Gold was deposited from a 2.5 DWT/Qt. gold electrodeposition solution at 0.7 V. When multicomponent nanowires were grown, the electrodeposition was done sequentially. The template remained in the cell, and the electrodeposition solution was changed after deposition of the first metal. Gold was grown first, followed by nickel. The wires grown with this technique have a radius $r = 170$ nm.

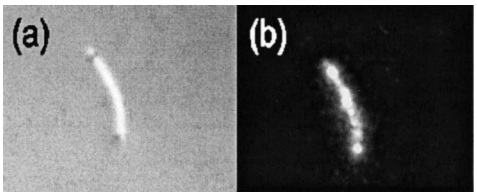

FIG. 1. Reflected light (a) and fluorescence (b) micrographs of a 6 μm long Au nanowire functionalized with the fluorescent porphyrin P-SAc.

After nanowire deposition, the copper layer was removed from the alumina membrane with a 0.5 M CuCl in 30% HCl aqueous etch. The membrane was then dissolved in 0.5 M KOH at 60 °C for 2 h with periodic ultrasonic agitation. Nickel and Ni/Au nanowires were collected from suspension by placing a permanent magnet on the lower side of the vial containing the suspension. The gold wires were collected by centrifugation at 14 000 rpm for 6 min. In both cases, the supernatant was decanted and replaced with 1.5 mL neat solvent. The nanowires were then resuspended by sonication, and this procedure was repeated until the solution *p*H was neutral.

III. CHEMICAL FUNCTIONALIZATION OF NANOWIRES

A. Experimental techniques

The materials used for the functionalization studies were Hematoporphyrin IX dihydrochloride (HemIX) [8,13-bis(1-hydroxyethyl)-3,7,12,17-tetra-methyl-21 H,23 H- porphine-2,18-dipropionic acid] (Aldrich), nonylmercaptan (Aldrich), and the thioacetate terminated porphyrin 5-[4-[2-[4-(S-Acetylthio)phenyl]ethynyl]phenyl]-10,15,-20- trimesitylporphyrin, abbreviated P-SAc.[18] The specific functionalization protocols used are described below. After reaction of the nanowires with the fluorescent porphyrins, the wires were rinsed as described herein until the supernatant was nonfluorescent.

For optical microscopy studies, the nanowires were spun out from suspension onto glass cover slips at 3000 rpm using a photoresist spinner. Fluorescence, bright-field, and reflection images were taken with the 60× objective of a Nikon TE200 inverted microscope equipped with a Orca 100 monochrome CCD camera. Fluorescence images were taken at a 7 s exposure time with a G-2E/C TRITC filter set, which gives excitation light in the wavelength of 525–555 nm and detects emission at 590–650 nm. Steady-state fluorescence and excitation spectroscopy measurements were performed on nanowire suspensions using a SPEX fluorolog spectrometer operating in front face mode.

B. Results and discussion

Thiols, dithiols, and thioacetates are well known to selectively bind to planar gold surfaces and gold nanoparticles.[19] Indeed, we find that reacting P-SAc with gold nanowires in methylene chloride for 24 h yields fluorescent nanowires that remain fluorescent after extensive rinsing using the procedure described herein. Figure 1 shows optical images of a single gold nanowire functionalized with P-SAc. Figure 1(a) shows a reflected light image, and Fig

Downloaded 13 May 2003 to 128.220.233.88. Redistribution subject to AIP license or copyright, see http://ojps.aip.org/japo/japcr.jsp

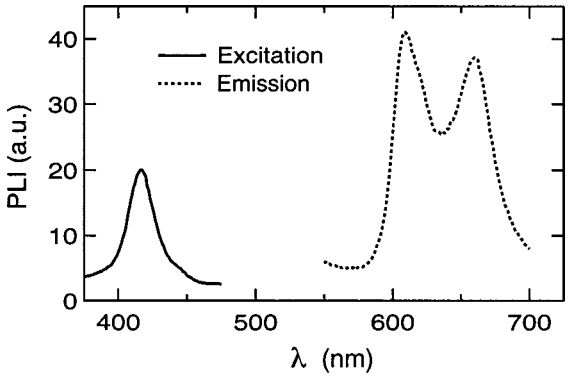

FIG. 2. Room-temperature fluorescence emission and excitation photoluminescence intensity spectra of P-SAc bound to gold nanowires in a 50/50 (v/v) hexadecane/octadecane solution.

1(b) shows a fluorescence image. The fluorescent layer was uniform in brightness and, presumably, coverage. Although it is likely that there is some quenching of the fluorescence due to proximity to the metal surface,[20,21] we nevertheless clearly observe fluorescence from these wires. Control experiments performed without the fluorescent porphyrins, but under otherwise identical conditions, resulted in nonluminescent nanowires.

Gold nanowires functionalized with P-SAc were suspended in a 50/50 (v/v) hexadecane/octadecane solution in a quartz cuvette and their steady-state fluorescence emission and excitation spectra were obtained, as shown in Fig. 2. After a few hours, the gold nanowires settled to the bottom of the cuvette and the fluorescence was lost indicating that the observed emission was from the functionalized nanowires. Steady-state fluorescence emission and excitation spectra recorded for P-SAc in fluid hexadecane/octadecane were in good agreement with those measured on the nanowire surface indicating that the porphyrins were bound to the gold surface with weak electronic coupling between the gold and the porphyrin through the mid-diphenyl-ethyne linkage.

In our previous work,[14] two-segment nickel-gold nanowires were selectively functionalized with a long-chain thiol, nonylmercaptan, and HemIX. The data were consistent with selective binding of the thiol to the gold segment, and of the carboxylic acid groups of the HemIX binding to the native oxide on nickel. In the initial studies, the concentrations of HemIX and the nonylmercaptan were both kept at 1 mM and were reacted with the nanowire surface at the same time. Here, we varied the thiol and porphyrin concentrations for these reactions, and investigated sequential functionalization procedures.

Two component nanowires that were 3/4 nickel and 1/4 gold were placed in a 1 mM HemIX and 1 mM nonylmercaptan ethanol solution for 24 h. The nanowires were then rinsed and isolated as just described. Figures 3(a) and 3(b) show reflection and luminescence images consistent with HemIX binding selectively to nickel. The concentrations of HemIX and nonylmercaptan in ethanol were systematically varied from 0.1 to 1 mM. Some typical spectroscopic data are shown in Fig. 4. The fluorescence data were quantified by averaging the integrated emission intensity along the length

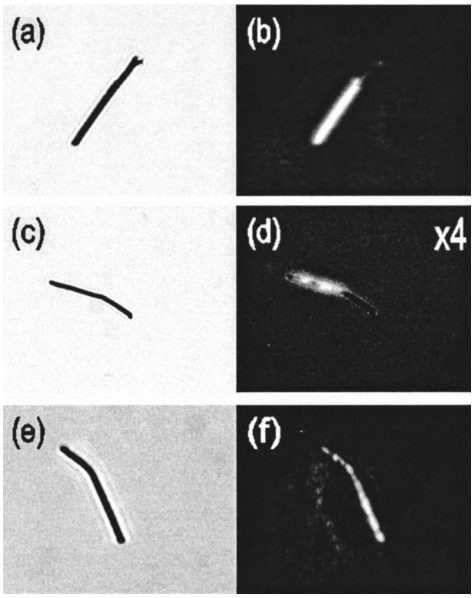

FIG. 3. Transmitted light (left-hand side column) and fluorescence (right-hand side column) micrographs of 14 μm nickel/gold wires that were functionalized with 1 mM HemIX and 1 mM nonylmercaptan. (a) and (b): Simultaneous reaction with both reagents. (c) and (d): Sequential reaction—HemIX first. (e) and (f): Sequential reaction—nonylmercaptan first.

of the nickel and gold segments. Results for the wires shown is given in Table I and can be qualitatively described as follows. A decrease in HemIX concentration results in a reduction of fluorescence intensity on the surface of the wire. A decrease of nonylmercaptan concentration causes no change in selectivity. The gold portion of the wire was nonfluorescent at 0.1 to 1.0 mM nonylmercaptan concentrations.

The nickel–gold nanowires were functionalized sequentially by first reacting the nanowires with one reactant in

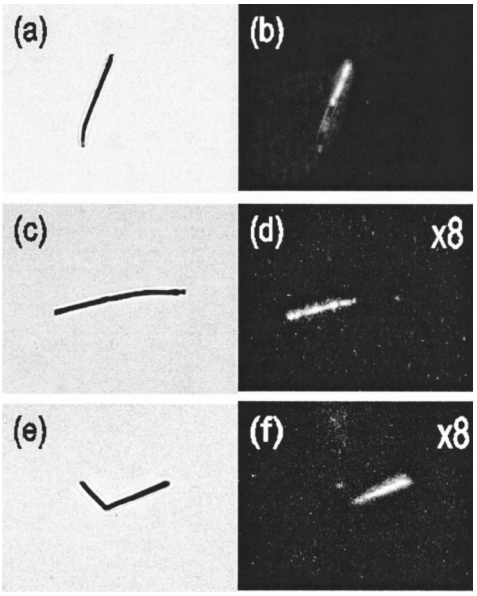

FIG. 4. Transmitted light (left-hand side column) and fluorescence (right-hand side column) micrographs of nickel/gold wires that were functionalized with solutions of varying concentrations. (a) and (b): 1 mM HemIX and 0.1 mM nonylmercaptan. (c) and (d): 0.1 mM HemIX and 1 mM nonylmercaptan. (e) and (f): 0.1 mM HemIX and 0.1 mM nonylmercaptan.

Downloaded 13 May 2003 to 128.220.233.88. Redistribution subject to AIP license or copyright, see http://ojps.aip.org/japo/japcr.jsp

TABLE I. Relative fluorescence intensities for Au/Ni nanowires. All reactions were performed for 24 h in ethanol.

Figure	Reaction conditions	Ni segment	Au segment
3(a) and 3(b)	1 mM HemIX 1 mM thiol	400±40	32±20
4(a) and 4(b)	1 mM HemIX 0.1 mM thiol	180±50	58±20
4(c) and 4(d)	0.1 mM HemIX 1 mM thiol	34±9	2±1
4(e) and 4(f)	0.1 mM HemIX 0.1 mM thiol	33±9	0.6±1
3(c) and 3(d)	1 mM HemIX first 1 mM thiol second	54±20	10±3
3(e) and 3(f)	1 mM thiol first 1 mM HemIX second	220±40	100±40

ethanol solution for 24 h and then, after rinsing, reacting them with the other reactant for 24 h. Examples of the resulting spectroscopic data are shown in Figs. 3(c)–3(f). Nanowires that were functionalized with HemIX first and then nonylmercaptan second [Figs. 3(c) and 3(d)] had no detectable fluorescence on the gold segment. There was however, a lower fluorescence intensity on the nickel segment than there was for wires functionalized simultaneously, suggesting that the thiol did displace some of the HemIX from the nickel segment. The nanowires that had been functionalized with nonylmercaptan first and then HemIX second [Figs. 3(e) and 3(f)] had significant fluorescence on both the gold and nickel segments. Integrated average emission data for these wires are given in Table I.

Taken together, the simultaneous and sequential functionalization of nickel–gold nanowire studies are consistent with literature reports that have shown strong gold–thiol and carboxylic acid–metal oxide interactions[19] and weak binding of thiols to oxidized nickel surfaces[22] and carboxylic acids to gold.[23] The advantage of the simultaneous functionalization approach is that the more thermodynamically favorable thiolate–gold and carboxylate–nickel oxide interactions are observed. The sequential functionalization procedure, on the other hand, appears to yield kinetic products and some undesirable substitution reactions.

IV. MAGNETIC TRAPPING OF NANOWIRES

The essential features of the magnetic trapping process are illustrated in Fig. 5. Magnetic nanowires in a suspension are allowed to settle onto a substrate that contains lithographically defined magnetic features. The local magnetic fields produced by these features influence the distribution of the nanowires on the substrate, and the nanowires are drawn into regions of strong local field gradients, such as the gap between two closely spaced micromagnets. If the gap is smaller than the size of the nanowires, then single nanowires can bridge the gap and become trapped.

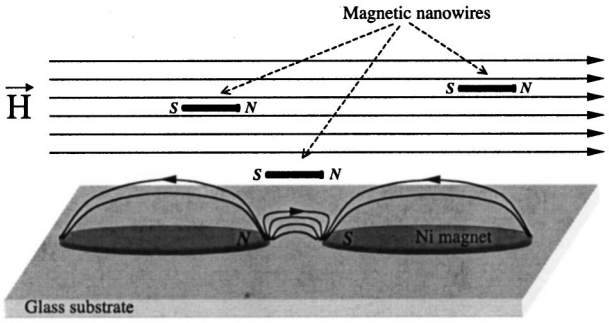

FIG. 5. Schematic representation of the magnetic trapping process. Magnetized nanowires are suspended in water, and a small external magnetic field H aligns them parallel to the long axis of lithographically fabricated magnets. Dipolar forces attract and trap the nanowires in the regions of strong local magnetic field between the poles of the magnets.

A. Experimental techniques

The magnetic trapping experiments were done using Ni nanowires of length $L=10\,\mu$m. The micromagnets used for trapping were patterned from Ni films on glass substrates, using photolithography, thermal evaporation, and lift-off processing. They were elliptical in shape, with a major axis of 80 μm, minor axis of 8 μm, and a thickness of either 50 or 100 nm. The ellipses were made in pairs, with a gap $g=6\,\mu$m between ellipses within a pair. A 5 nm thick Cr underlayer was used to promote adhesion of the Ni to the glass substrate. Examples of pairs of Ni micromagnets are shown in Fig. 6. Prior to the trapping experiments, the ellipses were magnetized in a 1 kG field, oriented parallel to their long axis. Measurements with a SQUID magnetometer indicate that this produces an average remnant magnetization in the ellipses of 135 Oe, 28% of the room temperature Ni saturation magnetization.

Magnetic trapping was carried out with nanowires suspended in water at $T=35\,^{\circ}$C. To limit interwire interactions in the suspensions, the experiments reported here were done with dilute nanowire concentrations of <200 wires/mm^3. The magnetic trapping process was monitored by video microscopy.

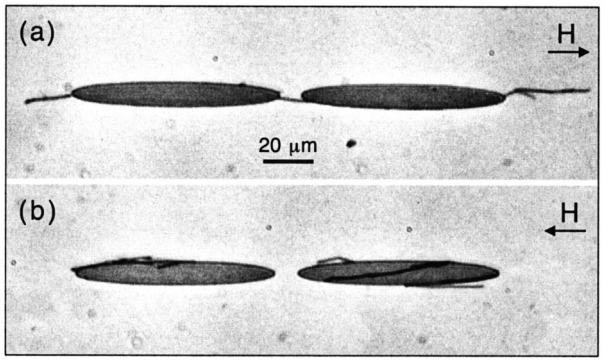

FIG. 6. Effect of an external magnetic field $H=10$ Oe on magnetic trapping. (a) Preorienting the dipole moments of the nanowires parallel to the moments of the elliptical micromagnets produces trapping in the gaps. (b) Preorienting moments of the nanowires antiparallel to the moments of the micromagnets repels the nanowires from the gaps.

Downloaded 13 May 2003 to 128.220.233.88. Redistribution subject to AIP license or copyright, see http://ojps.aip.org/japo/japcr.jsp

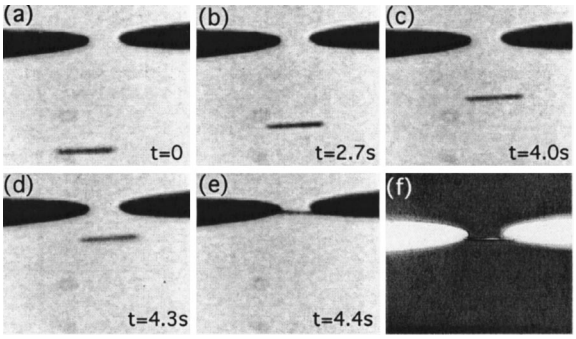

FIG. 7. (a)–(e) Video microscopy images showing trapping of a 10 μm Ni nanowire by elliptical Ni micromagnets in a 10 G external field oriented parallel to the magnetic moments of the micromagnets. (f) Reflected light micrograph taken after drying.

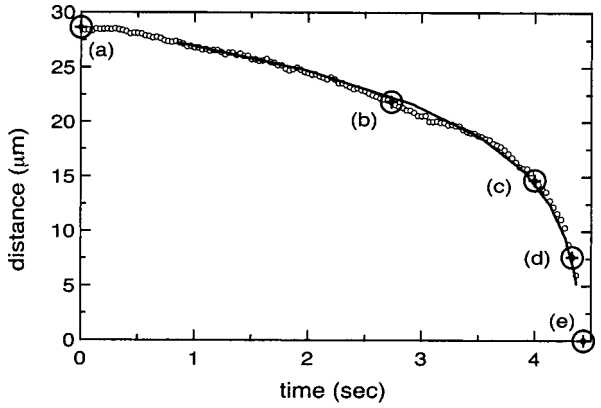

FIG. 8. Distance from center of nanowire to the center of the gap between the micromagnets in Fig. 7. The large circles show the positions of the images in Figs. 7(a)–7(e). The solid line is a fit based on Eq. (1).

B. Results and discussion

The trapping process is enhanced by the application of a small uniform magnetic field (2–20 G) parallel to the long axis of the ellipses, which preorients the suspended nanowires, as indicated in Fig. 5. This further reduces aggregation of wires in the suspension, and large numbers of single wires reach the bottom of the cell. More importantly, by aligning the dipole moments of the wires with the poles of the micromagnets, the configuration for trapping in the gaps is optimized. In the absence of this aligning field, the nanowires are attracted to the edges of the ellipses, roughly decorating the dipolar field lines. Trapping events in this case are quite rare. When the field is applied, the wires are repelled from the bodies of the ellipses and concentrate at the ends, producing trapping in the gaps as well as the formation of chains at the free ends, as shown in Fig. 6(a).

The influence of the external field is confirmed by reversing its direction, so that the suspended nanowires are prealigned antiparallel to the magnetic moments of the ellipses. In this case, the nanowires are repelled from the ends of the ellipses and are never trapped, but are instead attracted to the bodies of the ellipses, as shown in Fig. 6(b).

Figures 7(a)–7(e) show five video frames from a trapping event. Figure 7(f) shows a reflected light micrograph of the trapped wire after removal from the chamber and drying. The position of the wire was determined from each video frame using commercial object-tracking software (Igor Pro, Wavemetrics, Inc.). The distance from the center of the wire to the center of the gap between the two ellipses is shown in Fig. 8. The large circles in Fig. 8 show the positions of the five video frames in Fig. 7.

The slow initial motion of the wire and its rapid increase in speed as it approaches the trap are characteristic of the motion of the nanowire under dipole–dipole forces.[13] This motion occurs at very small Reynolds number $\mathrm{Re}<10^{-5}$ and, hence, the wires dynamics are dominated by viscous drag, with the velocity given by $\mathbf{v}=\mathbf{f}_M/D$, where $\mathbf{f}_M$ is the force on the wire due to the pair of micromagnets, and D is its drag coefficient. Analysis of events such as that shown in Fig. 7 where the wire is close to the perpendicular bisector of the axis of the gap allow us to assess the elements needed to model the trapping dynamics accurately. This is because here the torque on the wire due to the micromagnets is small, and the equation of motion reduces to a one-dimensional expression $dz/dt=f(z)/D$, where z is the distance from the center of the wire to the center of the gap. Treating the wire and the juxtaposed poles of the two ellipses as a pair of antialigned point dipoles is not adequate, as much of the motion occurs in a regime where the far-field condition $z \gg L$, g is not satisfied. However, we have shown in studies of the dynamics of nanowire–nanowire interactions in similar suspensions[13,24] that for distances large compared to the wire radius r, the wires are very well approximated by extended dipoles with magnetic charges $\pm Q_w = \pm M_w \pi r^2$ separated by L, with M_w as the magnetization of the wire. Somewhat more crudely, the poles of the ellipses may be modeled in a similar way, with effective magnetic charges Q^* separated by a distance g^*. For a wire moving along the perpendicular bisector of the gap, this gives

$$f(z) = -2Q_w Q^* z\left[\left(z^2+\left(\frac{L-g^*}{2}\right)^2\right)^{-3/2} - \left(z^2+\left(\frac{L+g^*}{2}\right)^2\right)^{-3/2}\right], \quad (1)$$

where we have neglected the $<5\%$ contribution from the far poles of the ellipses that are not visible in Fig. 7.

The resulting equation of motion may be integrated numerically to obtain the inverse of $z(t)$, $t(z)$. This allows data such as those in Fig. 8 to be modeled based on two parameters, g^* and $K=D/2Q_wQ^*$. This yields a good description of the motion of the wires over much of its range, as illustrated by the solid line in Fig. 8. For the event shown, we obtain $K=1.9(1)\times10^8\,\mathrm{cm}^4/\mathrm{s}$ and $g^*=20.8(1)\,\mu\mathrm{m}$. From the expression for the drag coefficient of a cylinder moving perpendicular to its axis near a wall,[25] we expect $D \approx 10^{-4}\,\mathrm{g/cm\,s}$. The wires are known to have remnant magnetization $M_w \approx 330\,\mathrm{Oe}$,[16] which yields. $Q_w = 3\times10^{-7}\,\mathrm{Oe\,cm}^2$, and from the measured remnant magnetization of the ellipses, we estimate $Q^* \approx 10^{-6}\,\mathrm{Oe\,cm}^2$. These values yield a calculated value $K_{\mathrm{calc}} \approx 2\times10^8\,\mathrm{cm}^4/\mathrm{s}$, in good agreement with the measured value of K. Such an analysis could clearly be improved, however, by a more detailed de-

Downloaded 13 May 2003 to 128.220.233.88. Redistribution subject to AIP license or copyright, see http://ojps.aip.org/japo/japcr.jsp

scription of the magnetization of the ellipses, either through micromagnetic modeling or through measurements with a magnetic force microscope.

V. SUMMARY

The experiments in this article have established results that will be of considerable use in the further development of multifunctional magnetic nanowires for biotechnology. The ability to control and chemically modify its surface is a crucial precondition for biological applications of any magnetic nanoparticle. The functionalization studies described here have pointed out the importance of both kinetic and thermodynamic considerations in derivatizing multicomponent nanowires. The magnetic trapping studies have demonstrated the efficacy of simple models to describe quantitatively the interactions of nanowires in suspension with localized sources of magnetic fields. This will potentially impact a broad range of applications, including biosensing, where the application of force and accurate positioning of biological entities is required.

ACKNOWLEDGMENTS

This work was supported by DARPA/AFOSR Grant No. F49620-02-1-0307, NSF Grant No. DMR-0080031, and by the David and Lucile Packard Foundation Grant No. 2001-17715. The authors thank Dr. J. Lindsey of North Carolina State University for providing the thiol-terminated porphyrin P-SAc.

[1] I. Safarik and M. Safarikova, J. Chromatography **722**, 33 (1999).
[2] C. Bergemann, D. Muller-Schulte, J. Oster, L. A. Brassard, and A. S. Lubbe, J. Magn. Magn. Mater. **194**, 45 (1999).
[3] K. Rudi, F. Larsen, and K. S. Jakobsen, Appl. Environmental Microbiol. **64**, 34 (1998).
[4] K. W. Peasley, Med. Hypothesis **46**, 5 (1996).
[5] L. R. Moore, M. Zborowski, L. Sun, and J. J. Chalmers, J. Biochem. Biophys. Methods **37**, 11 (1998).
[6] D. R. Baselt, G. L. Lee, M. Natesan, S. W. Metzger, P. E. Sheehan, and R. J. Colton, Biosens. Bioelectron. **13**, 731 (1998).
[7] F. C. MacKintosh and C. F. Schmidt, Curr. Opin. Colloid Interface Sci. **4**, 300 (1999).
[8] F. J. Alenghat, B. Fabry, K. Y. Tsai, W. H. Goldmann, and D. E. Ingber, Biochem. Biophys. Res. Commun. **277**, 93 (2000).
[9] *Scientific and Clinical Applications of Magnetic Microspheres*, edited by U. Häfeli, W. Schütt, J. Teller, and M. Zborowski (Plenum, New York, 1997).
[10] A. Fert and L. Piraux, J. Magn. Magn. Mater. **200**, 338 (1999), and references therein.
[11] C. Roberts *et al.*, J. Am. Chem. Soc. **120**, 6548 (1998); K. Heister *et al.*, Langmuir **15**, 5440 (1999); M. Baker *et al.*, *ibid.* **16**, 3288 (2000); J. Folkers *et al.*, *ibid.* **11**, 813 (1995).
[12] B. R. Martin, D. J. Dermody, B. D. Reiss, M. Fang, L. A. Lyon, M. J. Natan, and T. E. Mallouk, Adv. Mater. **11**, 1021 (1999).
[13] M. Tanase, L. A. Bauer, A. Hultgren, D. M. Silevitch, L. Sun, D. H. Reich, P. C. Searson, and G. J. Meyer, Nano Lett. **1**, 155 (2001).
[14] L. A. Bauer *et al.* (unpublished).
[15] *The Porphyrin Handbook*, edited by K. M. Kadish, K. M. Smith, and R. Guilard (Academic, San Diego, 2000).
[16] A. Hultgren, M. Tanase, C. S. Chen, G. J. Meyer, and D. H. Reich, J. Appl. Phys. **93**, 7554 (2003), these proceedings.
[17] M. Tanase, D. M. Silevitch, A. Hultgren, L. A. Bauer, P. C. Searson, G. J. Meyer, and D. H. Reich, J. Appl. Phys. **91**, 8549 (2002).
[18] D. T. Gryko, C. Clausen, K. M. Roth, N. Dontha, D. F. Bocian, W. G. Kuhr, and J. S. Lindsey, J. Org. Chem. **65**, 7345 (2000).
[19] A. Ulman, *An Introduction to Ultra Thin Organic Films, from Langmuir-Blodgett Films to Self-Assembly* (Academic, San Diego, 1991).
[20] S. H. Chen and C. W. Frank, Langmuir **7**, 1719 (1991).
[21] D. S. Karpovich and G. J. Planchard, Langmuir **12**, 5522 (1996).
[22] Z. Mekhalif, J. Riga, J.-J. Pireaux, and J. Delhalle, Langmuir **13**, 2285 (1997).
[23] Z. Zhang and T. Imae, Nano Lett. **1**, 241 (2001).
[24] C. L. Chien, L. Sun, M. Tanase, L. A. Bauer, A. Hultgren, D. M. Silevitch, G. J. Meyer, P. C. Searson, and D. H. Reich, J. Magn. Magn. Mater. **249**, 146 (2002).
[25] A. J. Hunt, F. Gittes, and J. Howard, Biophys. J. **67**, 766 (1994).

Downloaded 13 May 2003 to 128.220.233.88. Redistribution subject to AIP license or copyright, see http://ojps.aip.org/japo/japcr.jsp